Space weather and the direct use of Helioseismology for improved SW predictions

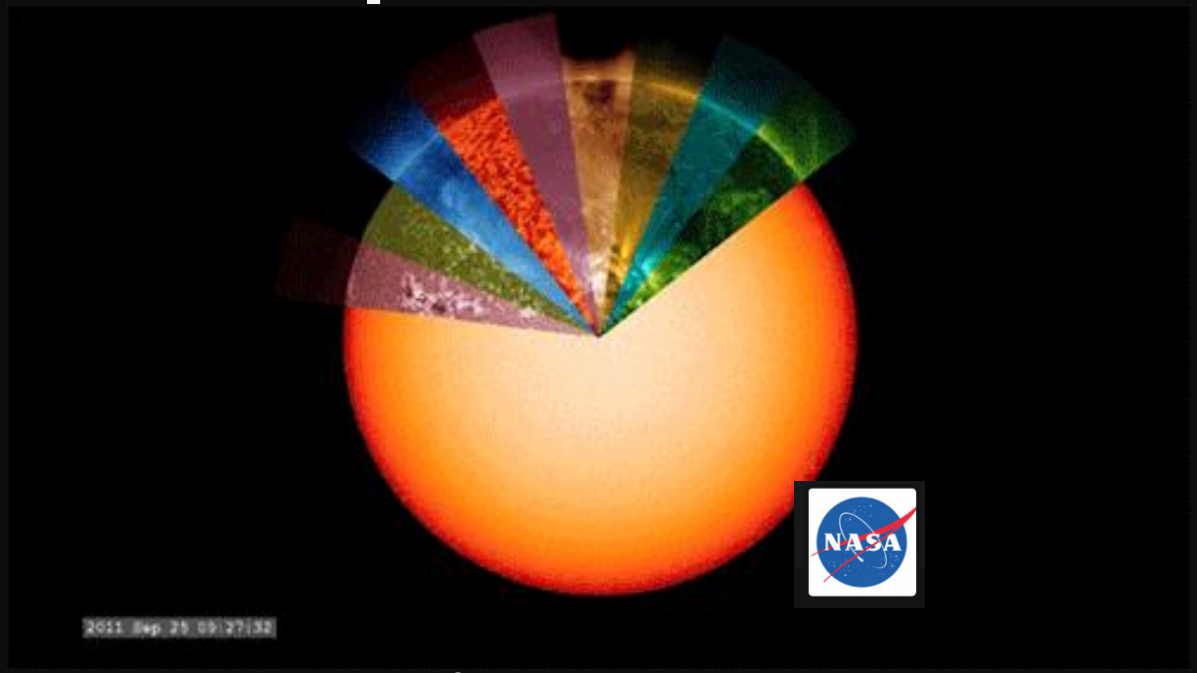

Alina Donea

Monash University

Solar Physics Group

OzSpace19

1969, 20th July

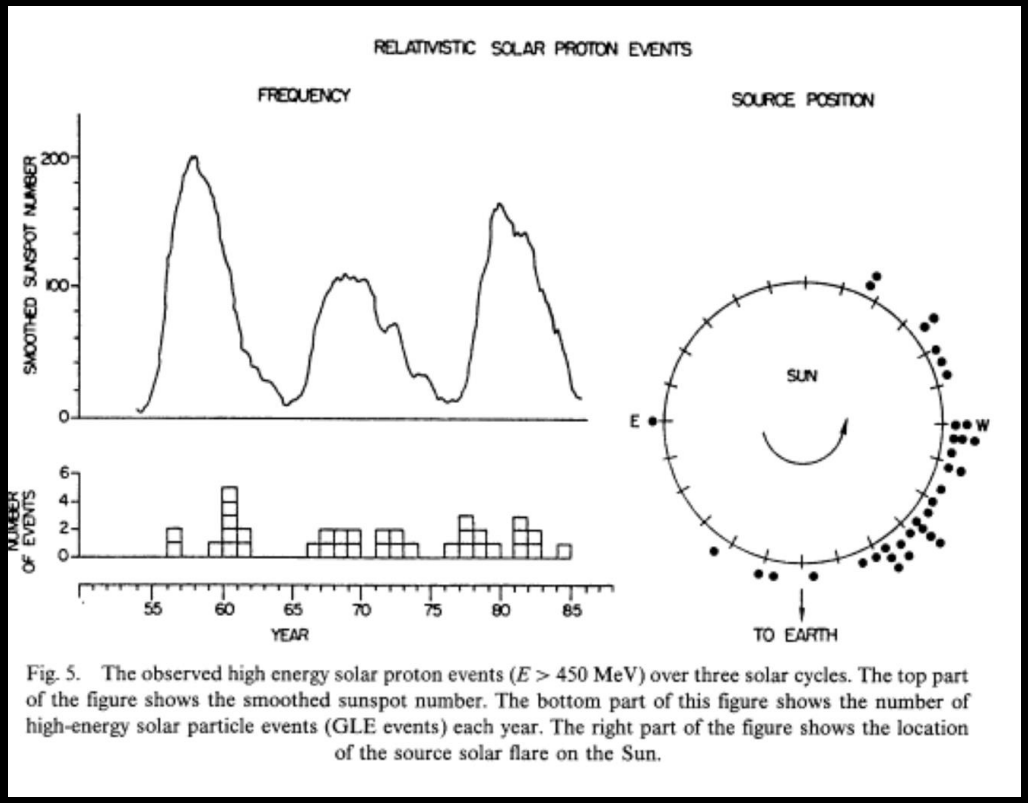

Fig. 5. The observed high energy solar proton events ($E > 450$ MeV) over three solar cycles. The top part of the figure shows the smoothed sunspot number. The bottom part of this figure shows the number of high-energy solar particle events (GLE events) each year. The right part of the figure shows the location of the source solar flare on the Sun.

NOTES

Solar Activity and Geomagnetic Storms 1969

Overall, solar activity decreased slightly during 1969 despite marked fluctuations. Considerable activity at the end of the first quarter was followed by a slow decline during the second half of the year.

The definitive annual Zürich sunspot number was 105·5, against 105·9 for the previous year; monthly means varied between 135·8 in March and 91·3 in September.

Table I

Zürich Mean Daily Sunspot Numbers (definitive) 1969

Jan.–June	104·4	120·5	135·8	106·8	120·0	106·0
July–Dec.	96·8	98·0	91·3	95·7	93·5	97·9

The number of sunspot groups with maximum corrected areas exceeding 500 millionths of the visible hemisphere fell to 42 (from 50 observed in 1968), including 12 with areas exceeding 1000 millionths.

The largest group, which attained a maximum area of 2700 millionths, crossed the disk between October 19 and November 1 (Central Meridian Passage October 26·1) in latitude 10° North.

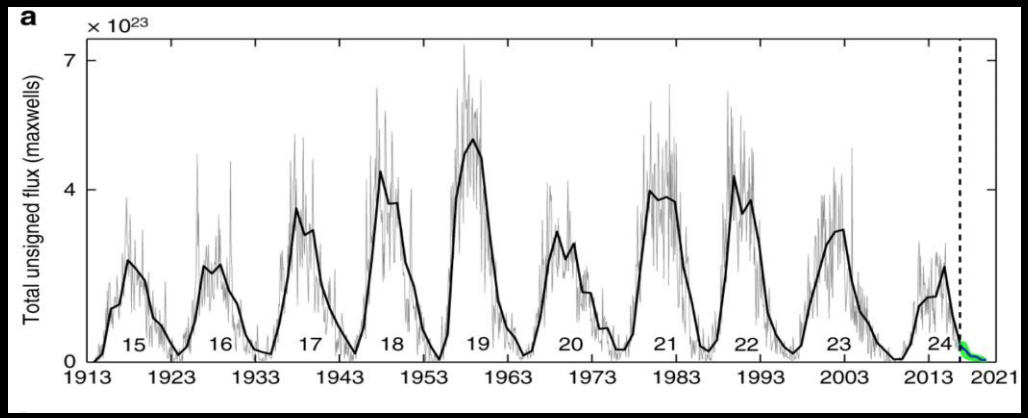

Shea, M. A. & Smart, D. F.(1990)
Prantika Bhowmik & Nandy (2018)

SOLAR FLARES
Confirmed

JULY 1969

OBSERVATORY	OBSERVED UT				LOCATION					DURATION	IMPORTANCE	OBS.		MEASUREMENTS					REMARKS
	DATE 1969 JULY	START	END	MAX. PHASE	APPROX. LAT.	APPROX. MER. DIST.	CENTRAL DISTANCE	McMATH PLAGE REGION	CMP DAY	MIN.		COND.	TYPE	TIME UT	MEAS. AREA Sq. Deg.	CORR. AREA Sq. Deg.	MAX. WIDTH Hα	MAX. INT. %	
GRP24370	19	1350	1418	1403	N06	W47	.729	10199	16.1	28	-N				.79				4 4 2 10
CATA	19	1350	1425D	1400	N08	W47	.729	10199	16.1	35D	-B			1400	1.16	1.70		204	
ONDR	19	1358E	1415D		N06	W48	.741	10199	16.0	17D	-F		V	1400			1.80		CDE
SACP	19	1359U	1419	1405	N05	W47	.729	10199	16.1	20D	-N		C		.42	.51			
AROS	19	1402E	1413		N06	W46	.717	10199	16.1	11D	-N		S						
	19	1915	1927	NO FLARE PATROL															
	19	1915	1927	NO FLARE PATROL															
	19	2041	2048	NO FLARE PATROL															
	19	2041	2048	NO FLARE PATROL															
GRP24371	20	0313	0332	0314	N25	W27	.543	10213	18.1	19	-F				1.17				2 2 2 5
CRON	20	0313	0321	0314	N25	W28	.554	10213	18.0	8	-N		C		1.00	1.20			
MANI	20	0319E	0342D		N25	W26	.532	10213	18.2	23D	-F	1		0320	1.34	1.59			
377 SANM	20	1836	1846	1839	N14	W59	.855	10199	16.3	10	--F	1	C		.15	.35			D 3
GRP24378	20	1936	2050	2023	S14	W28	.552	10209	18.7	74	--N				.83				2 1 1 3
HALE	20	1936	2050	2023	S14	W28	.552	10209	18.7	74	-N	2	C	2023	.83	1.00			
SANM	20	1937	1950	1943	S15	W29	.572	10209	18.6	13	-F	1	C		.32	.40			D
379 HALE	20	2011	2057	2038	S13	W89	1.000	10198	14.2	46	-N	2	C	2038	.41				2
GRP24380	21	0228	0243	0231	S17	W36	.666	10209	18.4	15	--B				.21				1 1 1 3
HALE	21	0228	0239	0231	S18	W35	.661	10209	18.5	11	-B	1	C	0231	.21	.30			
HALE	21	0230	0243	0233	S16	W37	.671	10209	18.3	13	-N	1	C	0233	.52	.70			
381 HALE	21	0326	0341	0327	N14	W65	.903	10199	16.3	15	--B	1	C	0327	.21				FW 3
388 HALE	21	2122	2135	2126	S15	W42	.721	10209	18.7	13	--B	2	C	2126	.15	.20			L 2

https://www.ngdc.noaa.gov/stp/space-weather/solar-data/solar-features/solar-flares/h-alpha/tables/1969/

Current conditions

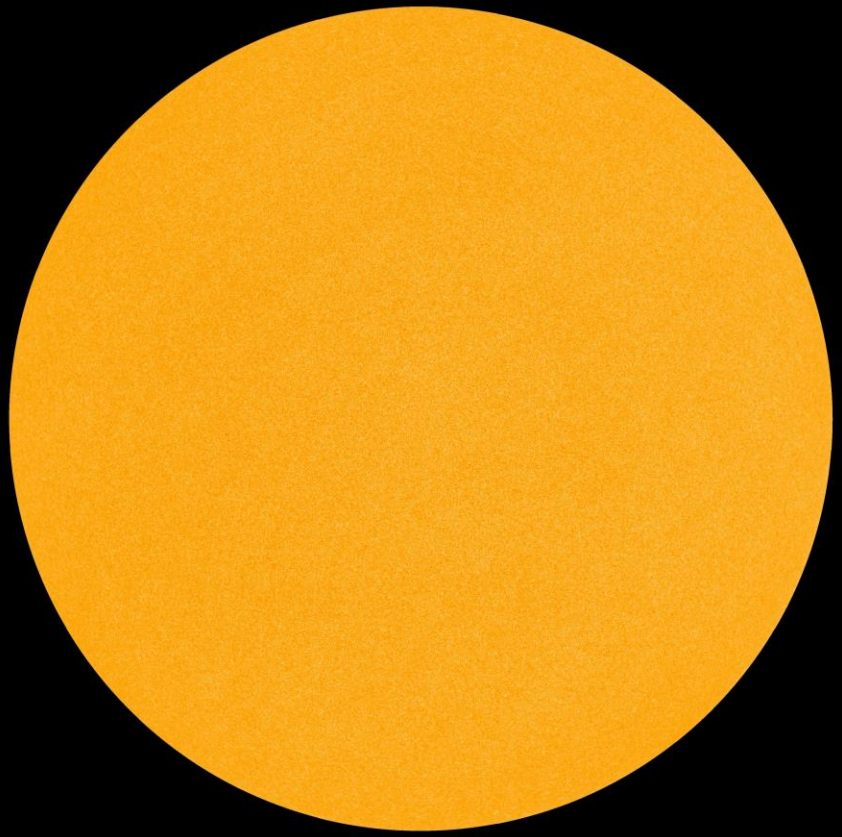

Solar wind
speed: 316.8 km/sec
density: 5.0 protons/cm3
more data: ACE, DSCOVR
Updated: Today at 1703 UT

X-ray Solar Flares
6-hr max: A7 1600 UT Jul21
24-hr: A8 0918 UT Jul21
explanation | more data
Updated: Today at: 1700 UT

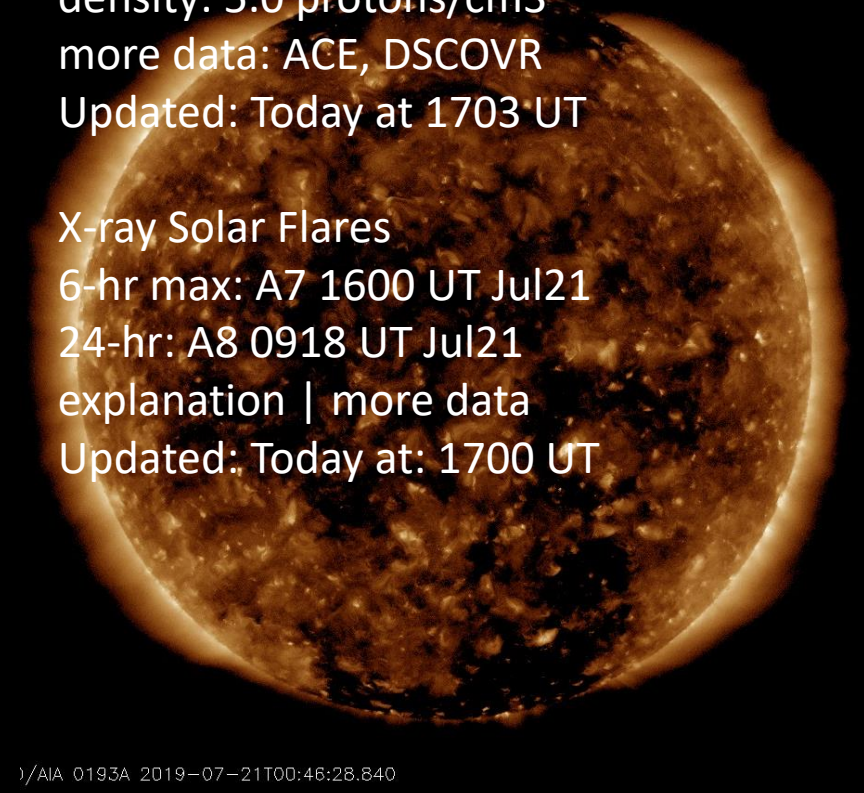

A stream of solar wind flowing from the indicated coronal hole should reach Earth on July 23-24, Credit: SDO/AIA

Solar activity
Large-scale view of initial coronal magnetic topology

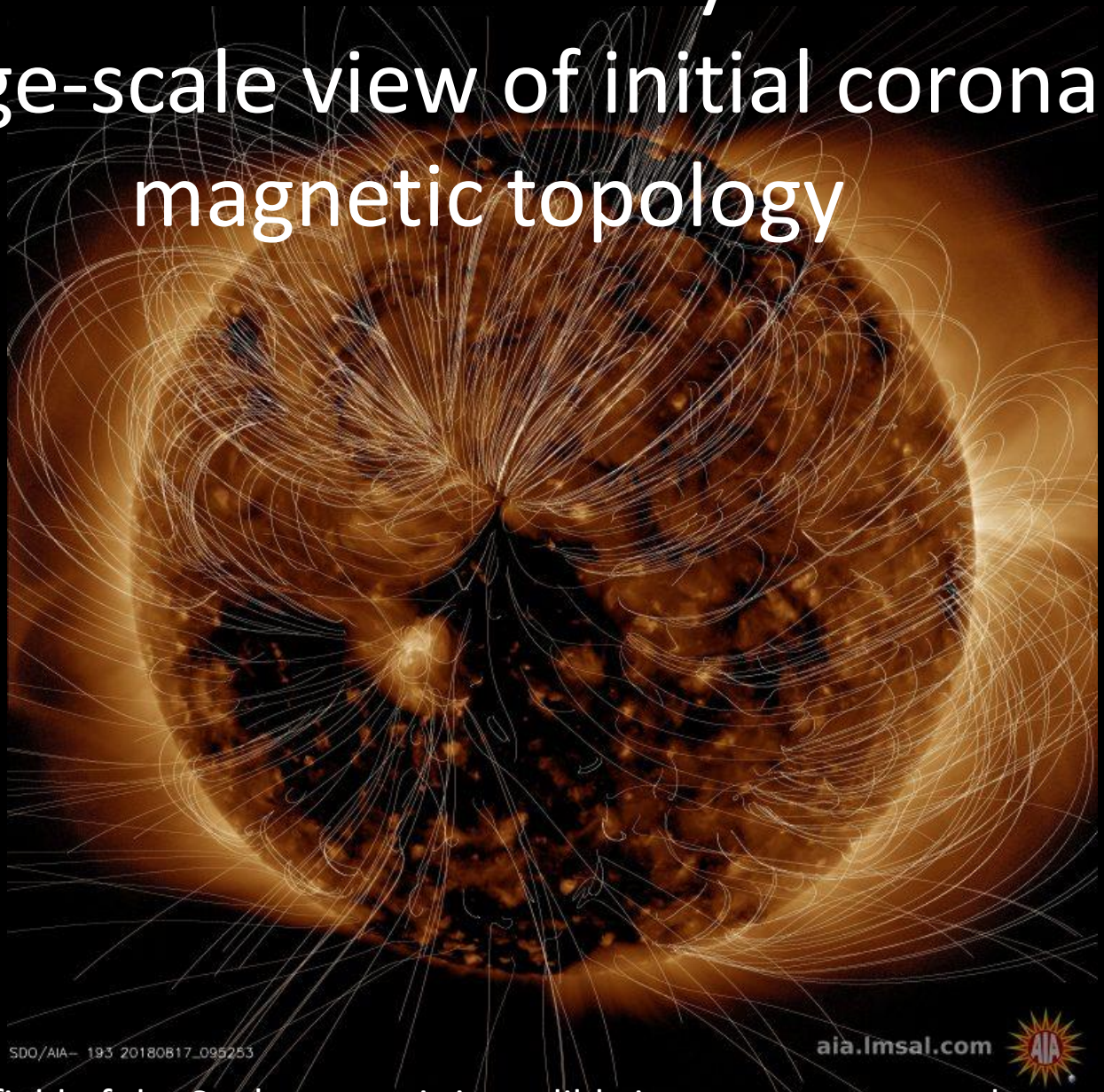

The magnetic field of the Sun's corona is incredibly important to our understanding of the solar atmosphere, and in turn, solar weather

The Sun's magnetic field can drive what is known as 'space weather' here on Earth

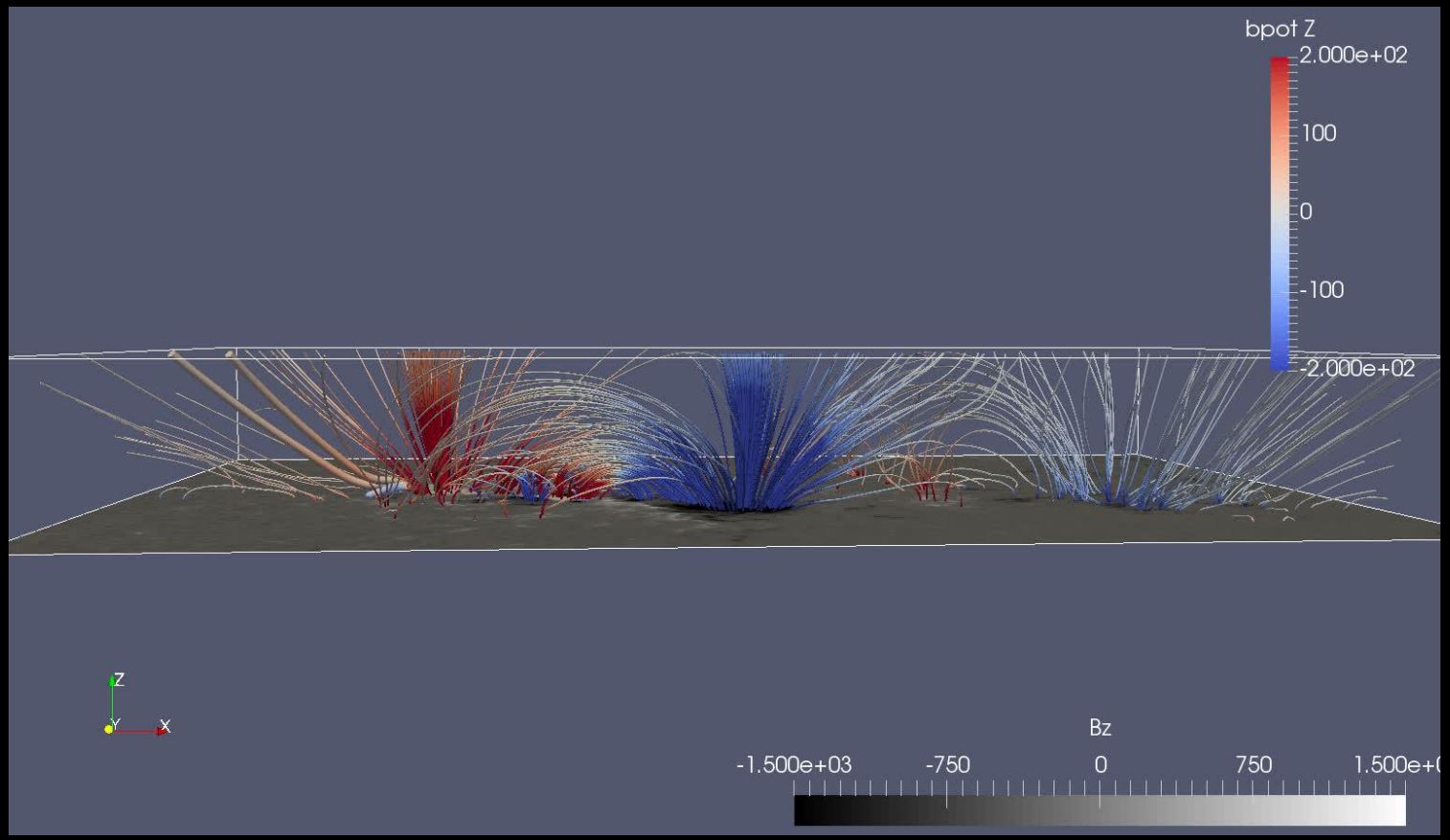

Paraschiv and Donea (2018)

Far side imaging of the Sun for space weather prediction:

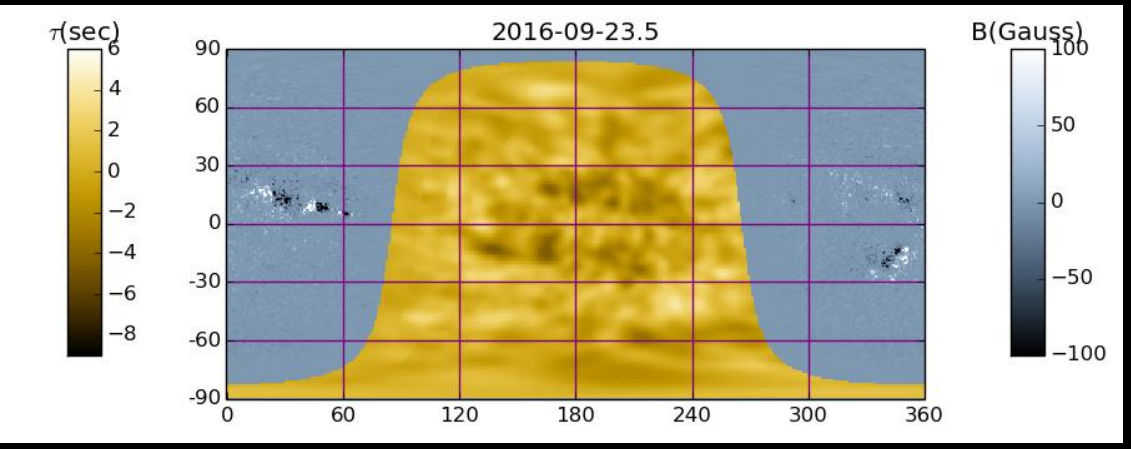

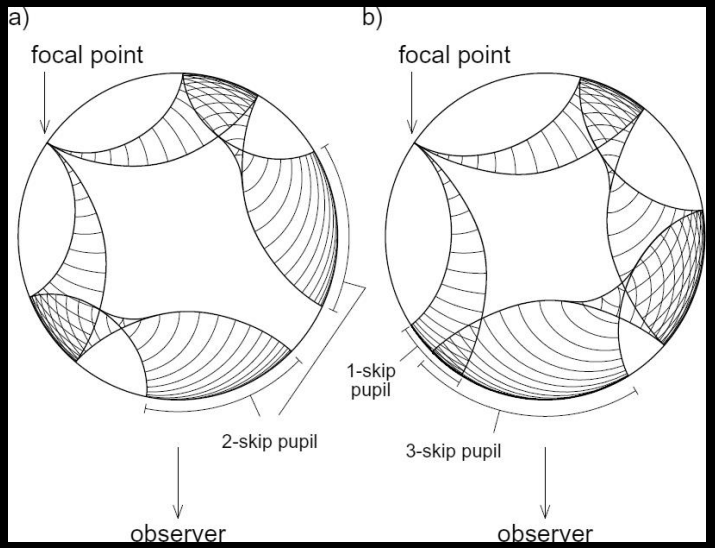

Phase shift between solar acoustic noise with periods of about five minutes embarking into the solar interior from the Sun's near hemisphere and its echos from respective locations in the far hemisphere

The ability of the far-side seismic monitor to detect and accurately locate the active regions in the far hemisphere that are of a major concern to space-weather forecasters is well established.

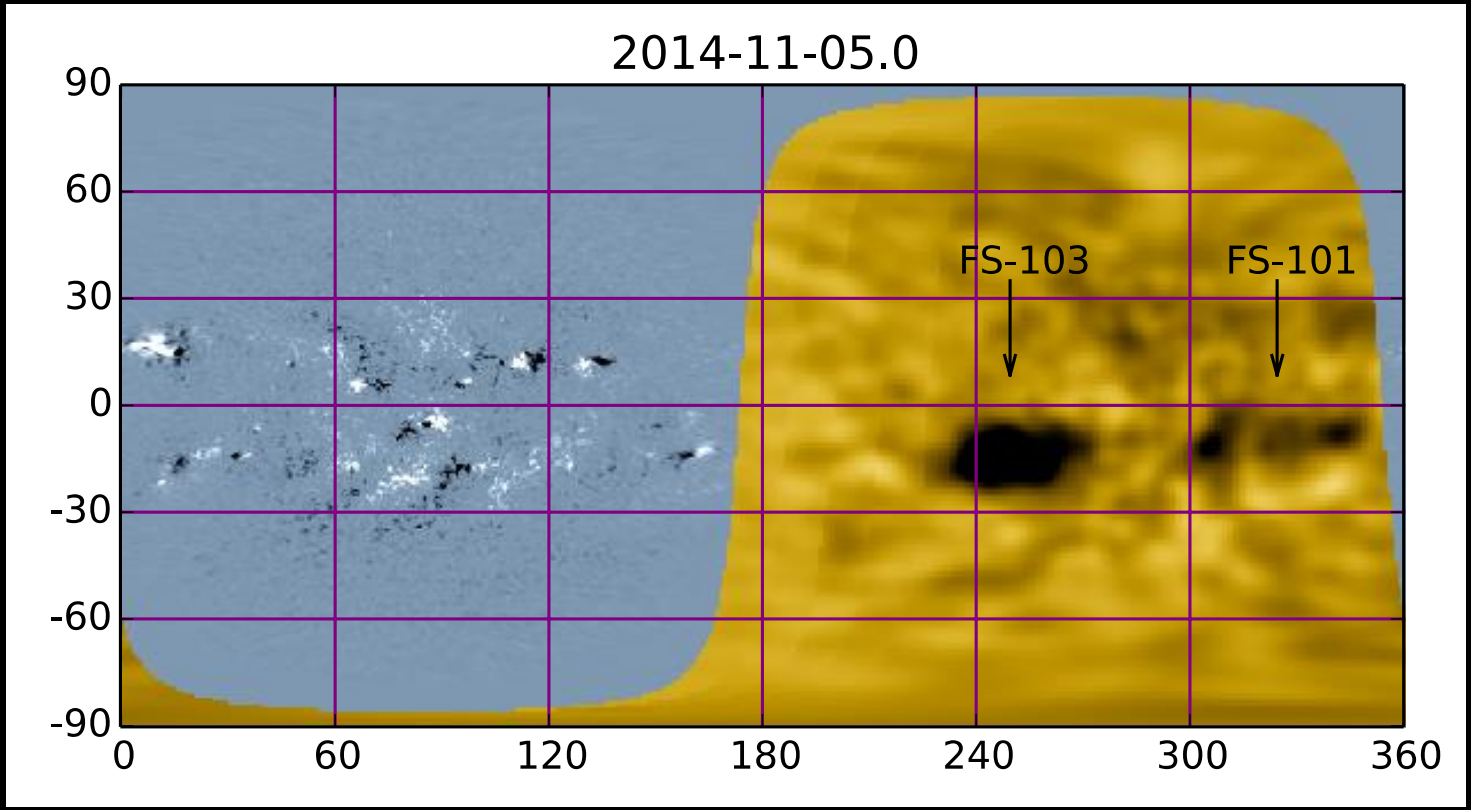

Composite map of the Sun on 2014-11-05.0 posted by the SDOs Joint Science Operations center

(see http://jsoc.stanford.edu/data/farside)

The Sun in visible, UV and EUV radiation on 2014-11-17

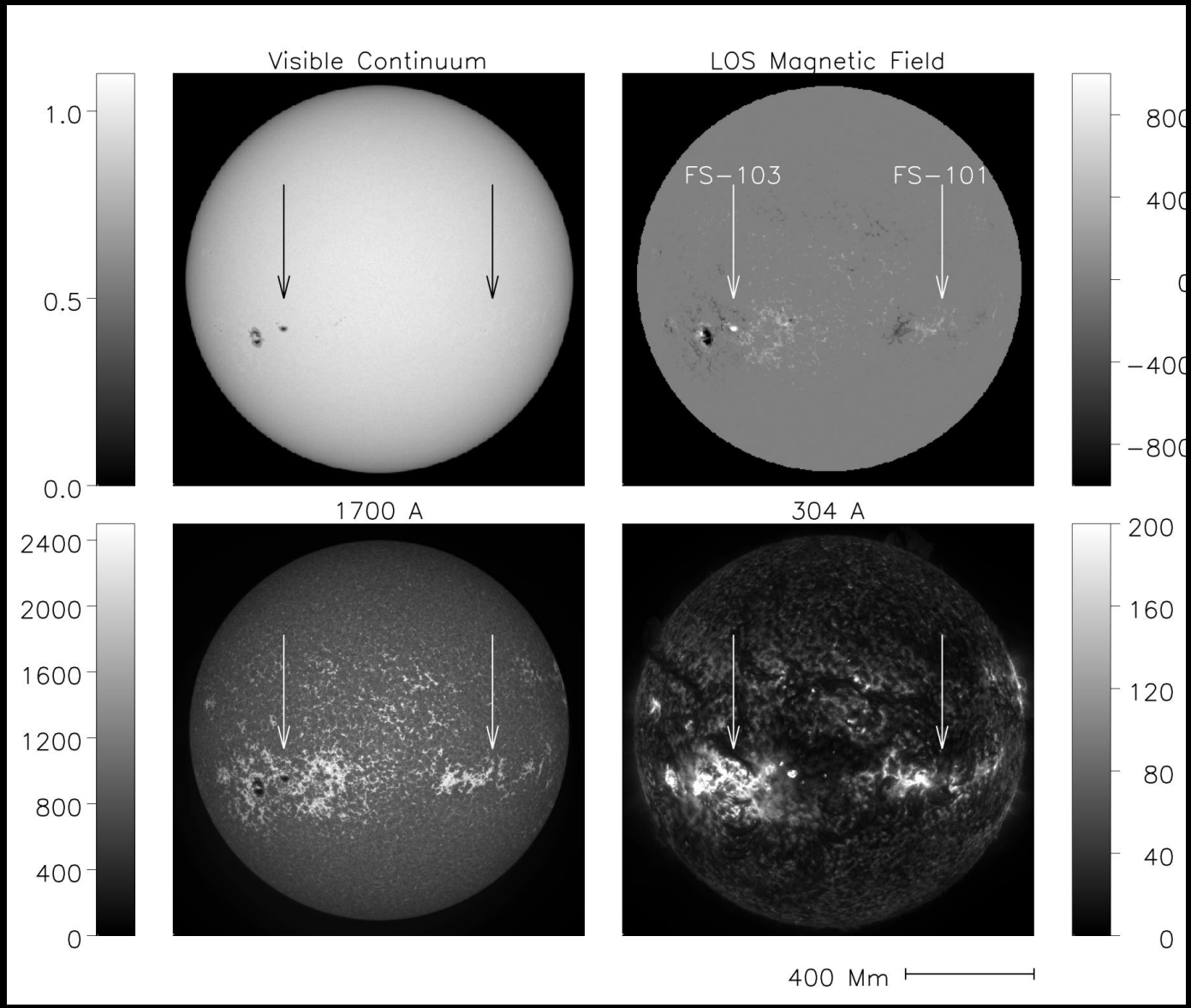

Magnetograms

- unfortunately, helioseismic signatures by themselves are insensitive to magnetic polarity.

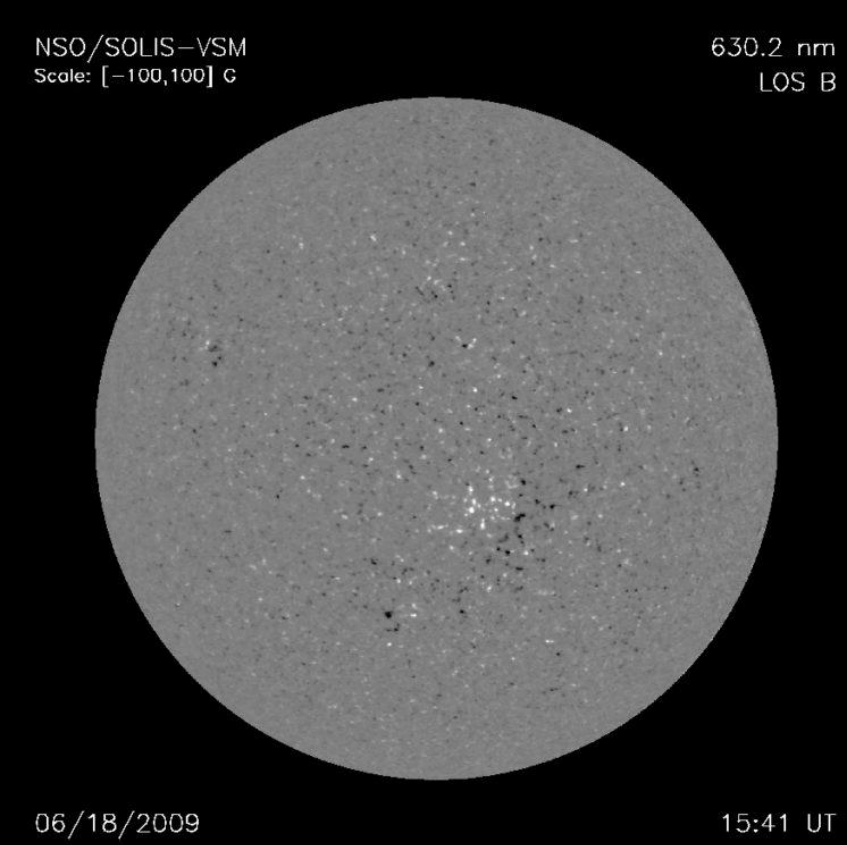

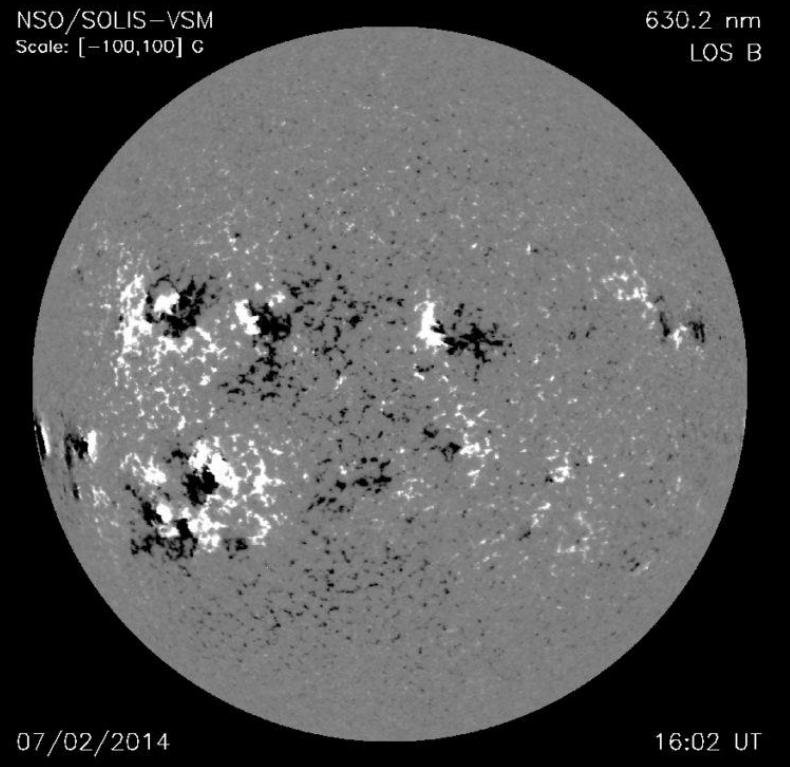

What do the helioseismic signatures actually tell us?

- Gonzalez et al. [2007] compiled statistics on the relationship between the strengths of helioseismic signatures of active regions in the Sun's far hemisphere and both their areas and magnetic fluxes when they subsequently appeared in the near hemisphere.

$$\mathcal{J}(\langle B^2 \rangle) \equiv h_0 \ln\left(1 + \frac{\langle B^2 \rangle}{B_0^2}\right)$$

$h_0 = -15.0$ sec, and $B_0 = 75$ Gauss.

$$H = \mathcal{J}(\langle B^2 \rangle)$$

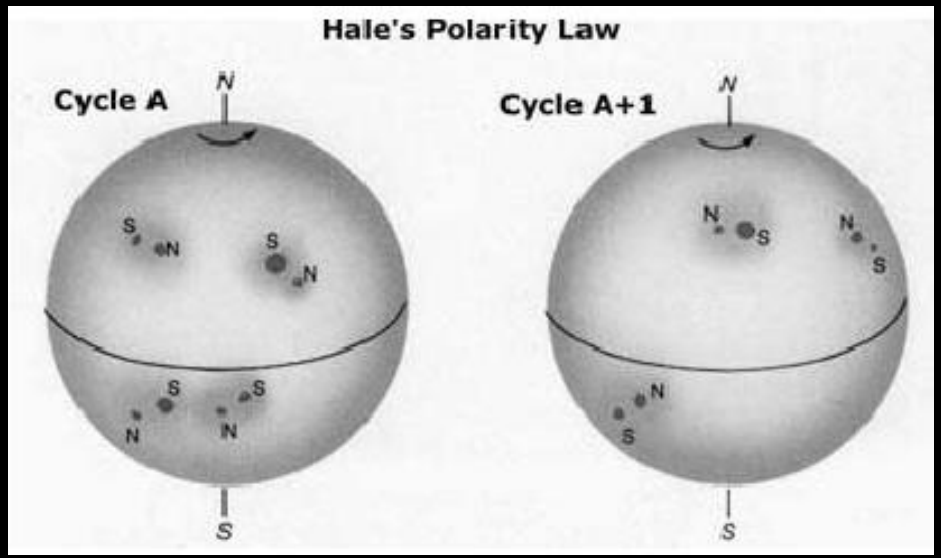

Donea ,Lindsey(2019) + Arge et al.(2013)

*H*elioseismic *EX*trapolator of *MA*gnetic-*P*olarity distribution (HEXMAP)

The relationship between helioseimic signatures and the magnetic configurations

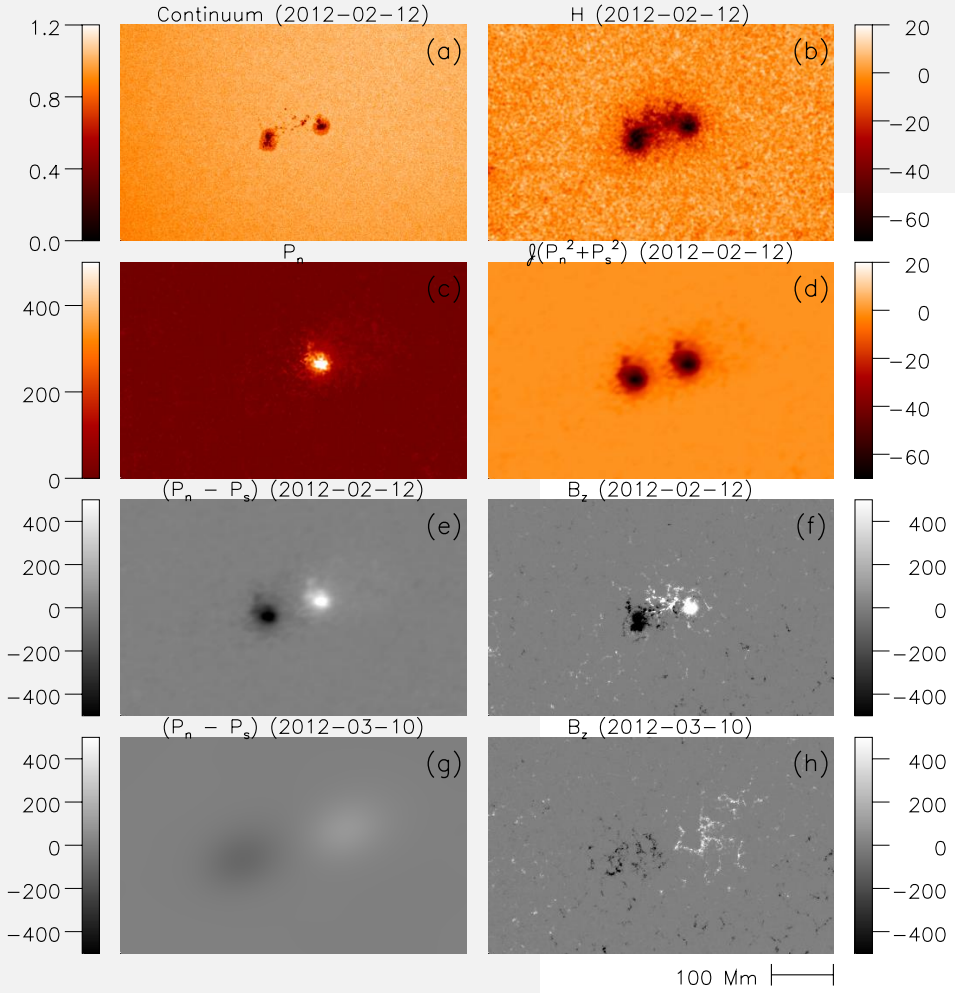

Donea, Lindsey (2019)

Magnetic Fields reduce Power in Local Acoustic Amplitude of Field Waves

- http://users.monash.edu.au/~adonea/farside.html

Solar farside magnetograms from deep learning analysis of STEREO/EUVI data

Taeyoung Kim et al 2019

deep learning model based on conditional generative adversarial networks (cGANs)

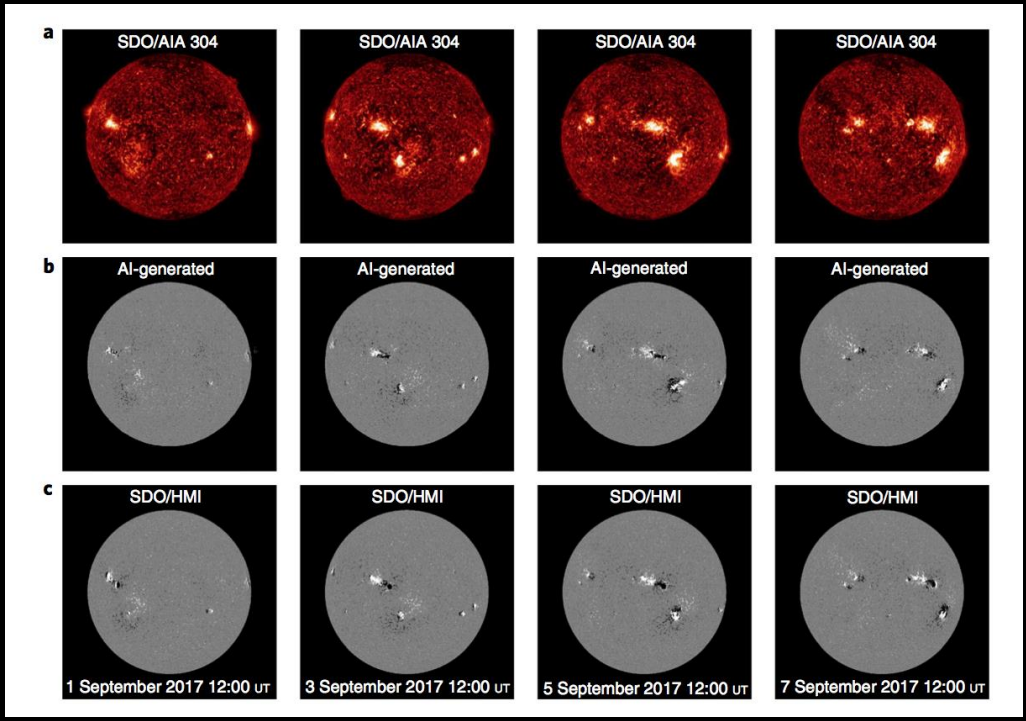

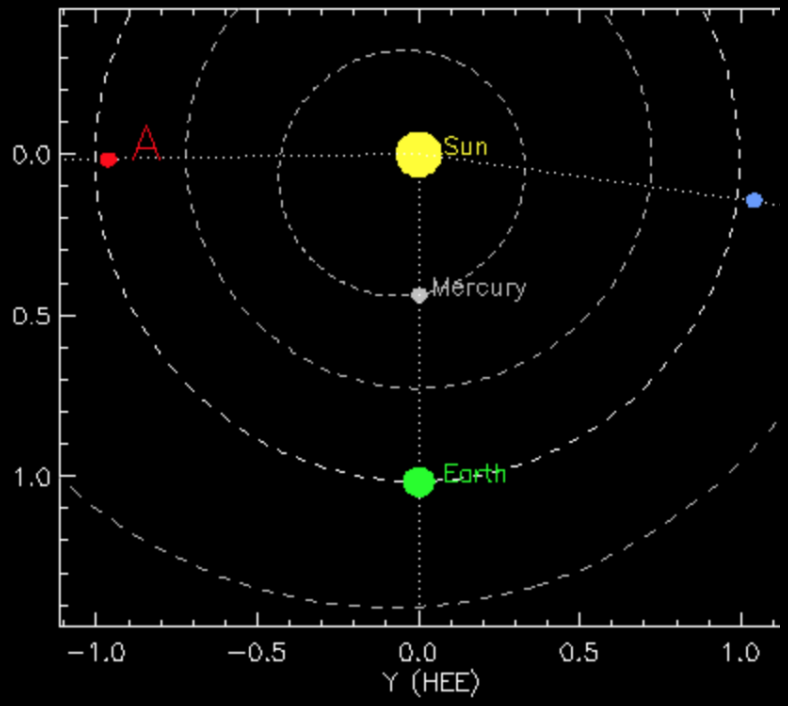

Comparison between HMI magnetograms and aI-generated ones from SDO/aIa 304-Å images.

Future Work

- Machine Learning for Recognition-Detection, Classification, Parametrization of Complex magnetic configurations:
- Where greater complexity gets interesting is when the different bipoles have different separations, **J**, both in direction and magnitude.

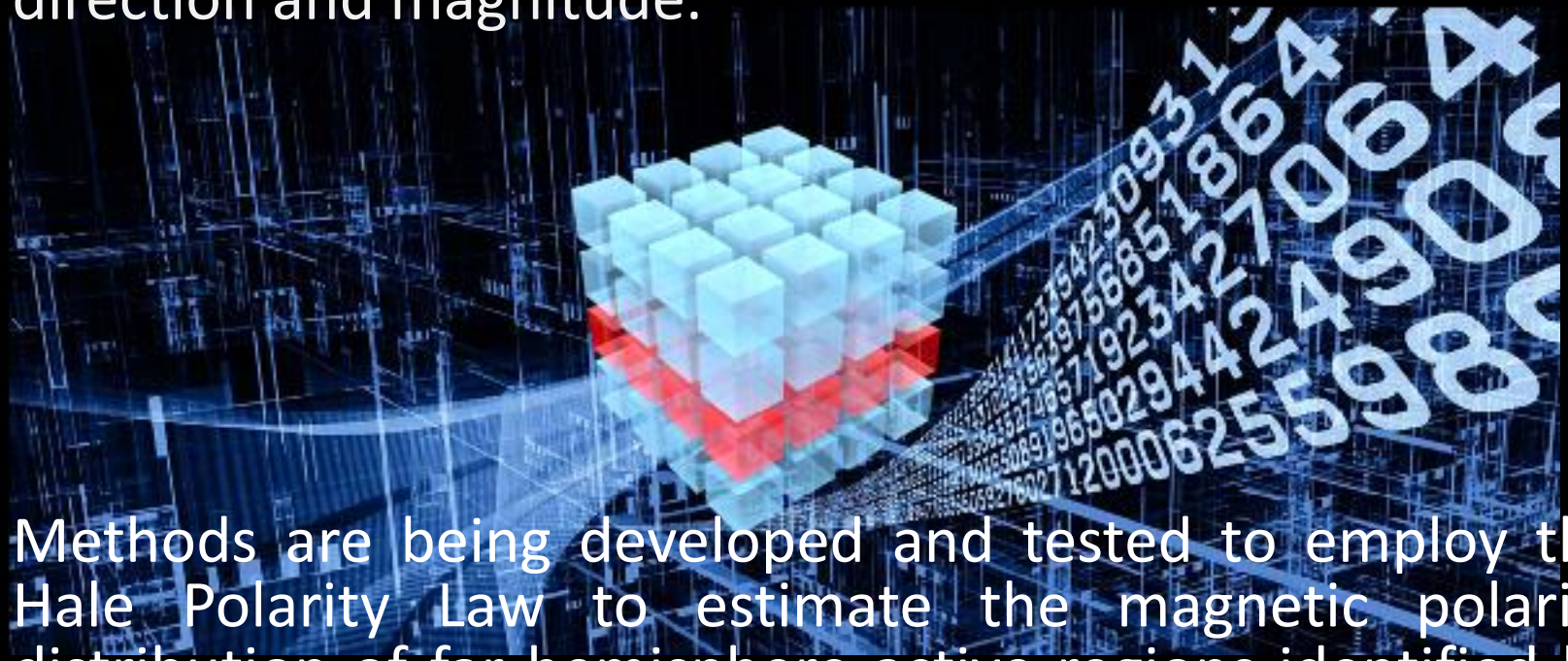

- Methods are being developed and tested to employ the Hale Polarity Law to estimate the magnetic polarity distribution of far hemisphere active regions identified by seismic observations.

Training of Data

- Space Weather Database of Notification, Knowledge, Information (DONKI) of NASA SpaceWeather Center,
- the Geostationary Operational Environmental Satellite(GOES)
- Space-Weather Heliospheric and
- Magnetic Imager Active Region Patches (SHARPs)

- CubeSats 10cm x 10cm x 30cm and weighing less than 10kg
- OneWeb, which has ambitions for a network of 2000 satellites orbiting 1200km above the Earth
- surprisingly difficult to get a handle on exactly how many satellites are orbiting the Earth right now. Thousands have been launched, but only about 1000-1500 have orbited or are functional at any one time.
- Current rules order that satellites must de-orbit and burn up within 25 years after their mission ends, but that’s too long for megaconstellations, Lewis (2017)
- Safely de-orbiting dead satellites or used rocket stages is a serious challenge, and space agencies around the world are working on solutions.
- titanium, which has a high melting point: about 1670 °C, aerodynamically shaped, making them more likely to reach the ground